**World Scientific**
www.worldscientific.com

# ELECTROFUSION OF MODEL LIPID MEMBRANES VIEWED WITH HIGH TEMPORAL RESOLUTION*

KARIN. A. RISKE[†], NATALYA BEZLYEPKINA, REINHARD LIPOWSKY and RUMIANA DIMOVA[‡]

*Max Planck Institute of Colloids and Interfaces, Science Park Golm, 14424 Potsdam, Germany*

[†] *Present address: Instituto de Física da Universidade de São Paulo, São Paulo, Brazil*
[‡] *Address for correspondence: Rumiana.Dimova@mpikg.mpg.de, fax: +49 331 567 9615*

The interaction of electric fields with lipid membranes and cells has been extensively studied in the last decades. The phenomena of electroporation and electrofusion are of particular interest because of their widespread use in cell biology and biotechnology. Giant vesicles, being of cell size and convenient for microscopy observations, are the simplest model of the cell membrane. However, optical microscopy observation of effects caused by electric DC pulses on giant vesicles is difficult because of the short duration of the pulse. Recently this difficulty has been overcome in our lab. Using a digital camera with high temporal resolution, we were able to access vesicle fusion dynamics on a sub-millisecond time scale. In this report, we present some observations on electro-deformation and –poration of single vesicles followed by an extensive study on the electrofusion of vesicle couples. Finally, we suggest an attractive approach for creating multidomain vesicles using electrofusion and present some preliminary results on the effect of membrane stiffness on the fusion dynamics.

*Keywords:* Model membranes; giant vesicles; electrofusion; electroporation; membrane domains.

## 1. Introduction

Membrane fusion is a ubiquitous process in the life of all eukaryotic cells. For example, fusion is involved in the cell feeding cycle, where large molecules or food particles are encapsulated by the cell membrane in endosomes (endocytosis), which then fuse with cell lysosomes. After digestion, the secondary lysosomes have to fuse with the cell membrane to allow the export of waste (exocytosis). Another example is the fusion of synaptic vesicles, which is significant for cell communication. Membrane trafficking in the Golgi body also involves membrane fusion. Viral infection provides yet another example where

*Paper presented at the conference on "Bio-Systems," Berlin, June 26–29, 2006.

the membrane of the virus has to fuse with the cell membrane. These are just a few examples illustrating the ubiquity of fusion in cell processes. In the context of biotechnology, vesicle fusion can be employed to scale down the interaction volumes of chemical reactions and reduce it to a few picoliters or less. Thus, fusion of two vesicles of different content is an illustration for the realization of a tiny microreactor.[1,2] On the other hand, fusing two vesicles that are bounded by membranes composed of different molecules, allows us to study raft-like domains in membranes[3–7] as demonstrated at the end of this report.

In cells, the control over fusion is mediated by the so-called fusogenic proteins. One example is provided by SNAREs.[8] The main role of these proteins is believed to be (*i*) bringing two opposing membranes together by creating a transmembrane protein complex; and (*ii*) locally perturbing the lipid bilayer and, thus, triggering fusion. In vitro, visualization of membrane-related processes is possible using giant vesicles,[9,10] a convenient membrane system of cell-size dimensions. To accomplish the first step of bringing two target vesicles together, experimentalists have already developed tools like micropipettes[11,12] and optical tweezers.[13,14] An alternative approach is to apply alternating electric fields to the vesicle solution. Similar to cells,[15] vesicles orient and align in the field in pearl chains. For diluted vesicle dispersions, these fields can be used to bring two vesicles into close contact. The second step towards fusion consisting in local perturbations of the bilayer structure, can then be accomplished by initiating focal points of interaction, like creating transmembrane complexes, or by inducing tension in the membrane, for example by ion adsorption or by electric fields.  Chemists have demonstrated that fusion proteins can be mimicked by synthetic fusogenic molecules incorporated in the membranes.[16] This approach was recently applied in our lab where giant vesicles functionalized with such molecules were brought into contact by means of micropipettes and observed to fuse after local injection of lanthanide ions.[17] An alternative approach to induce vesicle fusion is based on electroporation of two vesicles in contact. This method was only briefly reported in a previous publication from our group.[17] In this article, we describe the observations made on vesicle electrofusion in more detail.

Video microscopy observations on fusion have been previously limited in spatial and temporal resolution to microns and milliseconds, respectively, while membrane fusion involves reorganization on length scale of the order of few tens of nanometers and occurs on sub-millisecond time scales.[18] Here, we report microscopy observation on the dynamics of the electrofusion process at high temporal resolution reaching time scales in the microsecond range.

The interaction of electric fields with lipid membranes and cells has been extensively studied in the last decades.[19–21] The phenomenon of electroporation and electrofusion is of particular interest, because of its widespread use in cell biology and biotechnology, see Refs. 20–22 and references therein. Strong electric pulses of short duration induce electric breakdown of the lipid bilayers when the critical transmembrane potential is reached. The membranes become permeable for a certain time, because of transient pores

across the bilayer, allowing the exchange of molecules. For cells, which are aligned in the field and in close contact, the poration can lead to fusion and the subsequent creation of multinucleated cells with new properties (hybridization); see e.g. Ref. 15 and the references therein. In addition, electro-poration and -fusion is often used to introduce molecules like proteins, foreign genes (plasmids), antibodies, drugs, etc., into cells. Even though a lot is known about the phenomenology of cell electrofusion, the mechanism of pore opening across the lipid bilayers and the dynamics of fusion neck expansion are still not fully explored. Experiments on giant vesicles made of lipids and polymers are of special relevance because their size is comparable to cells and allows for direct observation using optical microscopy. However, mainly elecroporation processes have been studied.[23–26]

In the present study we use a fast imaging digital camera to record phase-contrast microscopy images of giant lipid vesicles with a high temporal resolution, up to 30 000 fps (1 image every 33 µs). Our aim is to elucidate the mechanisms underlying vesicle electrofusion by accessing the vesicle dynamics on a sub-millisecond time scale. Qualitatively different types of fusion behavior of the vesicles are observed depending on whether salt is present or absent in the outer vesicle solution. In this work, we focus on fusion events recorded in the presence of salt, for which we observe two dynamic regimes. We discuss the corresponding characteristic timescales and their relationship to the mechanical and rheological properties of the membranes.

The paper is organized as follows. After introducing the experimental system in the Materials and Methods section, we first give an example of the response of a single vesicle to a strong electric pulse in the absence and in the presence of salt. Then we consider vesicle couples, which experience electrofusion under the same conditions. The expansion of the fusion neck is quantified and discussed in the next section. At the end, we present some preliminary observations on the fusion of two vesicles composed of two different lipid mixtures. To clarify the conditions for membrane poration and fusion, we discuss some basic relationships about the membrane response to electric pulses in the appendix.

## 2. Materials and Methods

### 2.1. *Vesicle preparation*

The lipids used for the vesicle preparation were (*i*) L-α-Phosphatidylcholine from egg yolk (Egg-PC) from Sigma (St. Louis, MO), (*ii*) 1,2-Dioleoyl-sn-Glycero-3-Phosphocholine (DOPC) and (*iii*) egg sphingomyelin (SM) from Avanti Polar Lipids Inc. (Alabaster, AL), and (*iv*) cholesterol (Chol) from Sigma (St. Louis, MO). DOPC and cholesterol were mixed in 8:2 ratio; occasionally, a fluorescent marker provided by 1,1'-dioctadecyl-3,3,3',3'-tetramethylindocarbocyanine perchlorate (DiIC$_{18}$) from Molecular Probes (Leiden, The Netherlands; excitation wavelength at 551 nm and emission wavelength at 569 nm) was added at concentration 0.1 mol %. SM and cholesterol were

mixed in 7:3 ratio and perylene from Sigma-Aldrich (Steiheim, Germany; with excitation wavelength at 440 nm and emission wavelength at 450 nm) was added at concentration 0.4 mol %. Giant unilamellar vesicles were prepared using the electroformation method,[27] for details see Ref. 28. Briefly, lipid dissolved in chloroform was spread on the surfaces of two glasses coated with Indium Tin Oxide, and then dried under vacuum for about 2 h to remove the organic solvent. The two glasses and a rectangular Teflon spacer of thickness 2 mm were assembled to form a chamber sealed with silicon grease. An alternating current (1 V, 10 Hz) was applied to the glass plates and the chamber was filled with sucrose solution. The voltage was gradually increased to 2.5 V. Vesicles with an average size of 20 μm and large polydispersity were observed after about 4 h. The vesicle samples prepared from DOPC:Chol and SM:Chol mixtures were grown in an oven at 65°C to assure that the lipid is in the fluid phase. The obtained vesicle solution was removed from the electroswelling chamber and diluted 40 times into an isoosmolar glucose solution. This created a sugar asymmetry between the interior and the exterior of the vesicles. Due to the differences in density and refractive index between the sucrose and glucose solutions, the vesicles were stabilized by gravity at the bottom of the chamber and had better contrast when observed with phase contrast microscopy. The osmolarities of the sucrose and glucose solutions were measured with the cryoscopic osmometer Osmomat 030 (Gonotec, Berlin, Germany) and carefully matched to avoid osmotic pressure effects. The conductivities of the sucrose and glucose solutions were measured with the conductivity meter SevenEasy (Mettler Toledo, Greifensee, Switzerland), and found to be $6 \pm 1$ and $4.5 \pm 1$ μS/cm, respectively. In some experiments, the vesicles were prepared in sucrose solutions containing up to 1 mM NaCl and diluted in isoosmolar glucose solution of up to 3 mM NaCl. Thus the conductivities of the internal and the external solutions varied between 5 μS/cm and 120 μS/cm.

## 2.2. *Microscopy observation*

For fast digital recording of the fusion process, we used phase contrast microscopy. When studying fusion of vesicles from two different populations (of different composition and differently labeled with a fluorescent marker) we used fluorescent microscopy to distinguish the vesicle type.

Fast digital video microscopy was performed with an inverted microscope Axiovert 135 (Zeiss, Germany) using 20× and 40× Ph2 objectives. A fast digital camera HG-100 K (Redlake Inc., San Diego, CA) was mounted on the microscope and connected to a PC. Image sequences were acquired at 20 000 and 30 000 frames per second (fps), with picture resolution of 2.75 pixels/μm and 1.68 pixels/μm, respectively. Sample illumination was achieved with a mercury lamp HBO W/2. Sample heating due to illumination was measured to be less than 2°C, thus not significantly changing the bilayer properties.

Fluorescence microscopy snapshots were acquired with a confocal laser scanning microscope Leica DM IRE2 (Leica Microsystems Heidelberg GmbH, Germany) using 40× Ph2 objective and laser excitation at 476 nm (Ar laser) and at 561 nm (DPSS laser).

Emission light was detected by photomultiplier tube in the spectral ranges $480 - 533$ nm (for perylene) and $564 - 654$ nm (for $DiIC_{18}$). Experiments were performed at room temperature. Electrofusion events were recorded nearly at the equatorial plane of the fusing vesicles, at approximately 1 image per 1.6 sec. For three-dimensional image projection of a vesicle, z-scans in 0.34 µm increments were taken through the vesicle and projected using the Leica Confocal Software.

The observation chamber, purchased from Eppendorf (Hamburg, Germany), consisted of a Teflon frame confined above and below by two glass plates through which observation was possible. A pair of parallel electrode wires (92 µm in radius) was fixed at the lower glass at a nominal distance of 500 µm (for details see Ref. 28). The vesicles stayed at the bottom of the chamber due to gravity. The chamber was connected to a Multiporator (Eppendorf, Hamburg, Germany), which generated square-wave direct current (DC) pulses. The pulse strength and duration could be set in the range $5 - 300$ V ($0.1 \pm 0.01 - 6 \pm 0.6$ kV/cm) and $5 - 300$ µs respectively. Time zero was defined as one frame before visible vesicle deformation occurred, as observed with the fast camera. Presumably, this time corresponds to the beginning of the DC pulse with an error of maximum 33 µs for acquisition speed of 30 000 fps or 50 µs for acquisition speed of 20 000 fps.

## 3. Deformation of Single Vesicles Subjected to DC Pulses

The effect of DC pulses on single vesicles was reported in detail elsewhere.[28,29] Briefly, the applied pulse creates a transmembrane potential (see Appendix for details) which deforms the vesicle. In the absence of salt, the vesicle attains a prolate shape, which quickly relaxes back to a spherical shape after the end of the pulse; see the sequence in Fig. 1a. The vesicle response and relaxation time are defined by the material properties of the membrane and the tension of the vesicle. Another criterion, that influences the vesicle response time, is the media conductivity, which sets the charging time of the membrane (see Appendix for definition). In addition, as recently reported[29] the conductivity of the external solution, and in particular the presence of salt, leads to qualitatively different shape responses of the vesicles. When the solution outside the vesicles contains a small amount of salt (~ 1 mM NaCl), unusual short-lived shape deformations, mainly cylindrical, are observed; see snapshots in Fig. 1b. The dynamics of the vesicle deformation in this case, as well as some plausible hypothesis explaining these deformations were discussed elsewhere.[29]
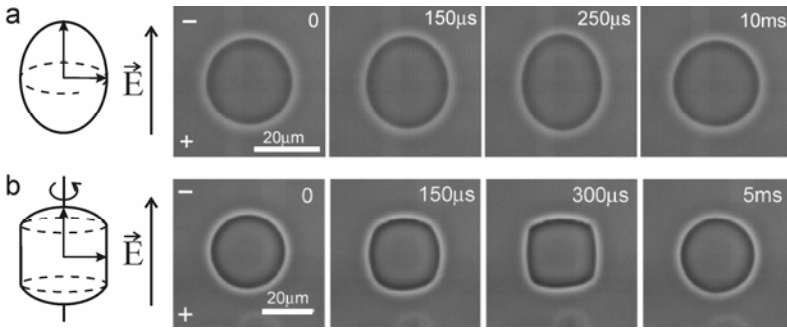
Fig. 1. Dynamics of vesicle deformation response to DC pulses. In the absence of salt the vesicles assume prolate shapes (a), while in the presence of salt in the vesicle exterior the vesicles become cylinders with spherical caps (b). In both cases the axis of symmetry is along the field direction (the electrode's polarity is indicated with a plus and a minus sign on the first snapshots). On the left side schematic illustrations of the deformations are given. (a) A vesicle of radius $R = 13.4$ μm in absence of salt, subjected to a pulse of strength 1 kV/cm and duration 200 μs. (b) A vesicle of radius $R = 14.6$ μm in 0.1 mM NaCl solution, subjected to a pulse of strength 2 kV/cm and duration 200 μs. The acquisition speed of the camera was 20 000 fps.

When the transmembrane potential applied exceeds some critical value, the membrane ruptures (see the Appendix for conditions of poration). Perforation of the membrane occurs when either of the following two conditions is satisfied:[28] (*i*) when the transmembrane potential exceeds a critical value of about ~ 1 V; or (*ii*) when the membrane tension approaches the lysis tension of the membrane (~ 5 dyn/cm for Egg-PC membranes). A clear sign that electroporation in a vesicle has occurred is the detection of optically resolvable macropores with diameters in the range $0.5 - 5$ μm (pores of smaller size cannot be optically detected). Their visualization is possible because of efflux of the inner sucrose solution, which under phase contrast microscopy appears darker than the external glucose solution. Thus, leakage leads to disruption of the bright halo around the vesicle. Some images of vesicles captured at the time of poration are given in Fig. 2. In general, membranes containing cholesterol are tougher (they rupture at higher lysis tension) and porate at stronger and/or longer field pulses. The pore lifetime for Egg-PC vesicles was found to be related to the membrane surface viscosity and edge energy.[28]
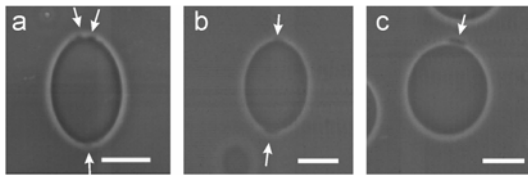


Fig. 2. Examples of electroporation of vesicles of different lipid composition: (a) Egg-PC vesicle, $R = 16.7$ μm at time $t = 200$ μs after applying a pulse of strength E = 1.25 kV/cm and duration $t_p = 200$ μs, (b) DOPC:Chol = 8:2 , $R = 18$ μm at $t = 600$ μs after applying a pulse of E = 1.4 kV/cm, $t_p = 200$μs, (c) SM:Chol = 7:3, $R = 20$ μm at $t = 300$ μs after applying a pulse of E = 1.3 kV/cm, $t_p = 200$ μs. Time $t = 0$ is defined as one frame before visible vesicle deformation occurred, as observed with the fast camera. The poration conditions (field strength and duration) depend on the membrane toughness and tension, and on the vesicle size (see the Appendix for details). Arrows indicate the leakage of internal solution from the vesicles, which is an indication for opening a pore on the membrane. The scale bar in all snapshots corresponds to 20 μm.

## 4. Electrofusion of Vesicle Couples

When exposed to a weak AC field, vesicles align in the direction of the field. This can bring two vesicles into close contact. Subsequent application of DC pulses to such a vesicle couple can lead to fusion when poration is induced in the contact area between the two vesicles. Figure 3 illustrates a possible fusion mechanism on the molecular scale. In the experiments reported here, we followed the evolution of the opening of the fusion neck diameter, $L$ (see Fig. 3c). The observations were performed using phase contrast microscopy, which does not resolve the fusion dynamics at the molecular scale as shown in Fig. 3, but at the micrometer scale. We observed two qualitatively different types of fusion behavior depending on whether salt was present in the vesicle exterior.
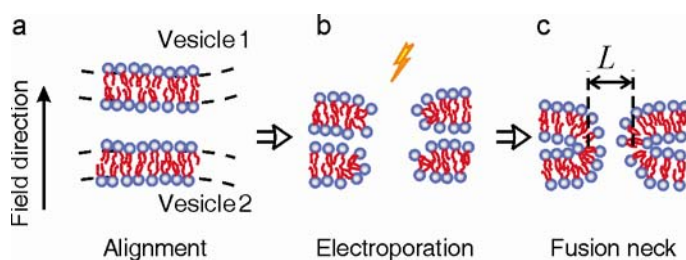


Fig. 3. Possible steps in electrofusion: (a) Alignment: two lipid vesicles are brought into contact via an AC field (the field direction is indicated with an arrow); only the membranes in the contact zone of the vesicles are sketched. (b) Electroporation: the two membranes are perforated by a short electric pulse. (c) Fusion neck formation: the lipids from the opposing bilayers mix, initiating the opening of the fusion neck of diameter "$L$".

In the *absence* of salt, fusion generally occurs simultaneously at several points in the relatively large contact zone created between the vesicles, as they are pushed together. This is easily deduced from inspection of the optical micrographs; see the example given in Fig. 4. Time $t = 0$ is defined as one frame before vesicle deformation is optically detected. When the two vesicles fuse at several contact points, the merged membranes close to form smaller vesicles. These contact-zone vesicles encapsulate some of the glucose solution external to the two initial vesicles and, thus, appear brighter on the snapshots (see arrows in the last two snapshots in Fig. 4). The membrane "loss" associated with the internalized small vesicles can be only roughly estimated from comparison between the total area of the two initial vesicles and the final fused vesicle. This comparison is not straightforward, as the shape of the resulting vesicle is not always spherical. The fused vesicle has a relatively large excess area as compared to a vesicle of the same volume but of spherical shape. Rough estimate based on the contact zone between the two initial vesicles formed during the pulse, gives for the membrane "loss" a value on the order of 2 – 3 % from the initial membrane area.
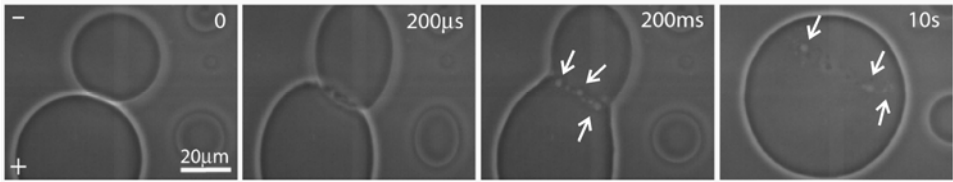
Fig. 4. Electrofusion of a vesicle couple (the vesicle radii are 18.2 μm and 24.7 μm) when exposed to a DC pulse in the absence of salt. The amplitude of the DC pulse was 1.6 kV/cm, its duration was 150 μs. The polarity of the electrodes is indicated with a plus (+) and a minus (−) sign. The starting time $t = 0$ corresponds to one frame before vesicle deformations due to the pulse are detected. In the last two snapshots, the fused vesicle contains an array of internal vesicles (bright spots) as indicated by the arrows. The image acquisition rate was 20 000 fps.

In the *presence* of salt in the solution outside the vesicles, the two vesicles generally form a smaller contact zone in-between, see Fig. 5. Note that in this case, the overall deformation corresponds to the cylindrical shapes as observed with individual vesicles in the presence of salt (see section 3). At these conditions, only one fusion neck (or a small number of such necks) is usually formed. Thus, we will focus on electrofusion in the presence of salt since this presumably enables us to resolve the dynamics of a single fusion neck.
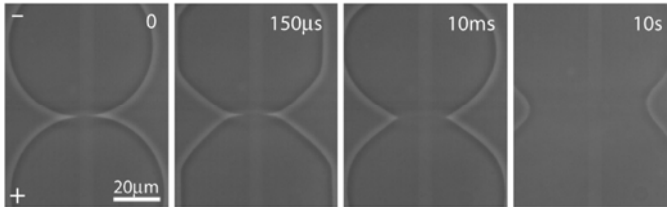


Fig. 5. Electrofusion of vesicle couple (the vesicle radii are 30.5 μm and 32.5 μm) when exposed to a DC pulse in the presence of 1 mM NaCl in the exterior solution. The amplitude of the DC pulse was 2.4 kV/cm, and its duration was 120 μs. The polarity of the electrodes is indicated with a plus (+) and a minus (−) sign. The image acquisition rate was 20 000 fps.

## 5. Time Evolution of the Fusion Neck

In Fig. 6 we give data on the expansion of the fusion neck diameter, $L$, (see Fig. 6a for definition) as a function of time, $t$. The data are collected from different vesicle couples, which fuse after being subjected to fields of various field strength and duration. A first inspection of Fig. 6b shows that the fusion process is surprisingly fast. Detailed image analysis of the fusion zone demonstrates that the opening of the fusion neck with a radius larger than ~ 10 μm takes place within the first several frames, e.g., within approximately 500 μs; see the early time data points in Fig. 6b. We emphasize that due to the flattening of the contact/fusion zone between the two vesicles (see second snapshot in Fig 5) in the initial few hundred microseconds the error in determining $L$ is relatively large (± 2 μm). Comparing the data obtained from different vesicle couples, one observes that they all exhibit a similar functional form for the time dependence of the fusion neck diameter. In

particular, two different dynamic regimes can be distinguished (note that the plot in Fig. 6b is semilogarithmic involving six decades in time). For clarity, in the inset of Fig. 6b we plot three of the data sets in linear time scale. A very fast expansion in the initial stage of fusion is detected, which slows down as the neck sizes reach some 20 micrometers. Even though both fusion stages (fast and slow) are observed for all vesicle couples, the neck diameter data differ significantly from one vesicle couple to another. However, we found out that these different neck diameters arise primarily because of the different vesicle sizes, at least in the early stage of fusion.

The fusion neck formed between two big vesicles will be larger than the one formed between two smaller vesicles. In Fig. 6c, we rescale the neck diameter $L$ by $(R_1+R_2)$ where $R_1$ and $R_2$ are the radii of the two vesicles before they were brought into contact. This leads to a collapse of the sets of data into a master curve for the time interval between 50 μs and 0.1 s (note that the initial few data points are determined with a larger error as already mentioned). The scatter of the data at later times is caused by very non-spherical shape changes for the fused vesicle. The fusion of the two vesicles leads to an *excess* area in the fused vesicle (as compared to the area of a vesicle of the same volume but of spherical shape). As the volume of the two initial vesicles is conserved after fusion, and the area "loss" is relatively small (< 3 %), the shape of the fused vesicle during the later stages of fusion can be very different from a sphere; therefore the rescaled neck diameter $L/(R_1 + R_2)$ can exceed 1 (Fig. 6c). As the fused vesicle, having acquired a lot of excess area, relaxes, it can spread on the bottom of the experimental chamber thus loosing its axial symmetry along the axis defined by the centers of mass of the two initial vesicles. Indeed, in several measurements it was necessary to refocus as the vesicle was flattening in the last few seconds of the fusion process. The shape of the fusion neck cross section is no longer perfectly circular but rather elliptical (with the long axis parallel to the chamber bottom). Because the fusion of different vesicle couples (implying both different sizes of the vesicles and different initial tensions) leads to different excess area in the product vesicle, the rescaling of $L$ does not lead to a collapse of the data into a single master curve at the later stages of fusion.

Irrespectively of the slight differences of expansion rates during the later fusion stages for the various vesicle couples, it is obvious that compared to the earlier times of fusion the neck expansion velocity slows down by more than two orders of magnitude. To understand the timescales involved in the two different stages of fusion, we consider some material properties of the fusing vesicles. In the early stage of fusion, the membrane tension is high, close to the lysis tension, since poration is a necessary condition for electrofusion (see the Appendix for details). Thus, the characteristic time in the early stage is mainly related to the relaxation of membrane stretching counterbalanced by the viscous dissipation in the membrane as the fusion neck expands.[17] In the later stage, the dynamics is mainly governed by the displacement of the volume $\Delta V$ of fluid around the fusion neck between the fused vesicles. The restoring force is related to the bending elasticity of the lipid bilayer. The corresponding decay time in this later stage can be

presented as $\tau_{late} \sim \eta \Delta V/\kappa$, where $\eta$ is the bulk viscosity of sucrose/glucose solution and $\kappa$ is the bending elasticity modulus of the membrane.

The displaced volume can be approximated with $\Delta V \sim R^3$, where $R$ is the average size of the fusing vesicles. For Egg-PC $\kappa \approx 10^{-19}$ J.[30,31] Thus for a typical vesicle size of $R$ = 15 μm, we obtain $\tau_{late} \sim 30$ s which provides the correct order of magnitude for the observations. The measured times for complete fusion of different vesicle couples as shown in Fig. 6c varied between about 10 and 30 seconds. Our dimensional analysis suggests that this scatter arises from the different sizes of the fusing vesicle couples, i.e., from the different values for the displaced liquid volume $\Delta V$. This conclusion is confirmed by some preliminary analysis taking into account the vesicle sizes. In addition, considering the inverse dependence of $\tau_{late}$ on the bending elasticity modulus $\kappa$, one can regulate the rate of fusion neck opening in the later stage by tuning the membrane stiffness. Indeed, as we will see in the preliminary experiments reported in the next section, the opening of the fusion neck can be accelerated and the data shifted to shorter times by an order of magnitude in time, if one uses vesicles whose membrane has higher stiffness, i.e. higher $\kappa$.
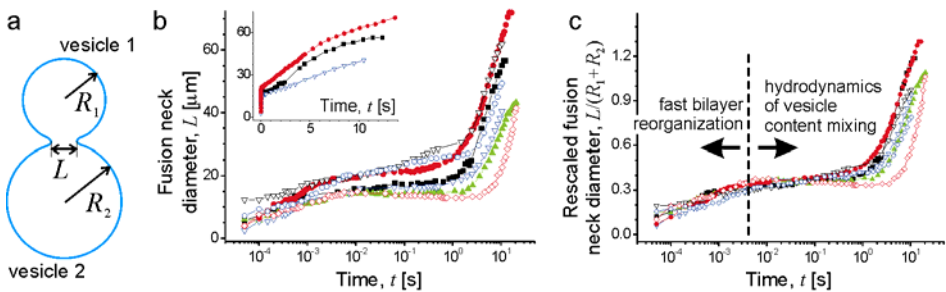


Fig. 6. Time evolution of the fusion neck. (a) A schematic illustration of fusion of two vesicles of initial sizes $R_1$ and $R_2$. The fusion neck diameter, $L$, is also indicated. (b) Data collected from seven vesicle couples of different sizes (between 10 and 25 μm in radius) fusing in presence of salt. The inset displays three of the data sets in linear time scale. (c) The fusion neck diameter rescaled by the sum of the radii of the fusing vesicles. The dashed line is a guide to the eye indicating the border between the two stages in the fusion dynamics.

## 6. Perspectives: Electrofusion of Vesicles of Different Composition

Finally, we present some preliminary results, which illustrate the application of our electrofusion protocol to more complex membrane systems. In particular, we consider the fusion of two vesicles that have different lipid composition. Recently, there has been much interest in raft-like lipid mixtures and domains in membranes.[4–6,32,33] The electrofusion of vesicles is a very attractive experimental approach for producing multicomponent vesicles of well-defined composition. For certain compositions and/or temperatures, multicomponent membranes can be quenched into a phase coexistence region leading to the formation of domains of different characteristics on the same vesicle.[3]

Even though giant vesicles have again been found to be a very suitable and handy system to study the phase separation and domain formation in "raft" mixtures,[4,6] the reader should be aware of the following concern. When giant vesicles are prepared from a multicomponent lipid mixture, the composition of the different vesicles in a batch can vary drastically depending on the individual history of the vesicles. For example, events like budding and pinching off of a part of the vesicle during the preparation and manipulation of the sample may lead to a vesicle composition rather different from the starting lipid mixture. Thus, electrofusion of two vesicles made of different lipids is an alternative and attractive way of arriving at a specific vesicle composition. An example for this procedure is shown in Fig. 7. Two vesicles made of different lipids and labeled with different fluorescent markers are subjected to a strong electric pulse and fuse. The resulting vesicle is made of two domains with areas corresponding to the sizes of the initial vesicles. Depending on the bilayer properties and the experimental conditions, the domains can exhibit interesting dynamics; in our example, one of the domains buds. The resulting vesicle composition can be located precisely in the Gibbs triangle (Fig. 7e) by measuring the domain areas. Thus, starting with two (or more domains produced by successive fusion) one can address the stability of such systems with respect to domain number and configuration.
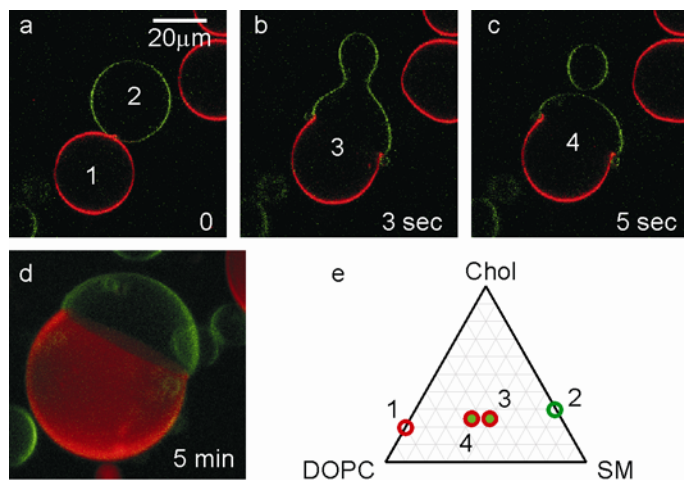


Fig. 7. Creating a multidomain vesicle by electrofusion of two vesicles of different composition as observed with fluorescence microscopy. The images (a-c) are acquired with confocal microscopy scans nearly at the equatorial plane of the fusing vesicles. (a) Vesicle 1 is composed of DOPC:Chol (8:2) and labelled with DiI-$C_{18}$ (*red*). Vesicle 2 is made of SM:Chol (7:3) and labeled with perylene (*green*). (b) The two vesicles were subjected to an electric pulse (6 kV/cm, duration 300 µs) and fused to form vesicle 3. (c) Right after the fusion, the SM-Chol membrane part (*green*) begins to bud forming a small daughter vesicle. (d) A three-dimensional image projection of a vesicle 4. (e) The numbered circles in the Gibbs diagram indicate the approximate composition of the vesicles marked with the same number as in the microscopy images.

Using our fast digital camera setup, we were also able to record the fusion of couples of vesicles of different composition. We used two populations of vesicles, DOPC:Chol

8:2 and SM:Chol 7:3, labelled differently so that the initial vesicles could be distinguished using fluorescence microscopy. The vesicles prepared from these lipid mixtures were in general smaller than those prepared from Egg-PC. This small size together with the difficulty to work with a selected pair of vesicles for fusion is currently the reason for low resolution of the image sequences acquired in the initial stage of fusion. However, our current data allows comparison of the fusion dynamics in the later stage between fusion of two Egg-PC vesicles and the fusion of a DOPC:Chol vesicle with a SM:Chol vesicle.

Two data sets corresponding to these two systems are given in Fig. 8. The fusion rates in the later stage of the two sets are very different. The Egg-PC vesicle fusion is almost 10 times slower compared to the fusion of the DOPC:Chol / SM:Chol couple. This is understandable if one considers the higher bending elasticity modulus of the cholesterol-containing membranes. Our dimensional analysis given in the previous section suggests that a larger bending rigidity $\kappa$ leads to shorter time scale $\tau_{late}$, and, thus, increases the fusion rate; see the slope of the plots in Fig. 8. To our knowledge, no data are available for the bending stiffness of membranes of the composition we used, but for membranes composed of DOPC:Chol and SM:Chol both in 1:1 ratio, the bending elastic modulus is known to increase several times compared to pure DOPC membranes.[34] Thus, the curvature caused by the fusion neck is quickly relaxed because of the higher membrane stiffness in the case of the cholesterol-containing membranes.
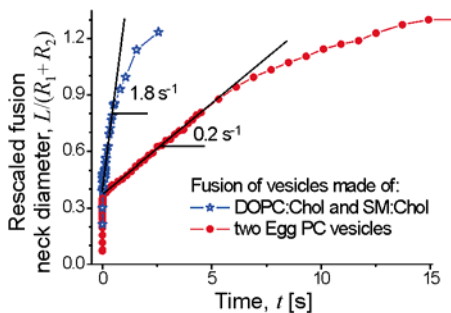


Fig. 8. Opening of the fusion neck measured during the fusion of two vesicles made of Egg-PC (closed circles) and the fusion a vesicle made of DOPC:Chol in 8:2 ratio with a vesicle made of SM:Chol in 7:3 ratio (open stars). In both cases, the fusion neck diameter $L$ was normalized by the sizes of the fusing vesicles. The slopes of the data at the later stage of fusion (solid lines) give the fusion rates indicated in the figure. The difference between these fusion rates is set by the different membrane stiffness and the vesicle sizes.

## 8. Concluding remarks

To summarize, using giant vesicles we were able to resolve electrofusion events with high temporal resolution. Until now, the limits of observation with optical microscopy were in the range of milliseconds. Using fast digital imaging, we were able to shift the resolution limit by about two orders of magnitude and study the fusion dynamics with microsecond resolution. To introduce the reader to electrophenomena on model

membranes, we first presented some observations on electro-deformation and –poration of single vesicles followed by an extensive study on the electrofusion of vesicle couples. Appropriate normalization of the fusion neck allowed us to collapse the experimental data from many fusion events into a master curve. The latter revealed two fusion stages – initially a fast one and later a slow one. The presented dimensional analysis suggests that the later stage of fusion is influenced by the membrane bending stiffness. Some preliminary experiments on fusion of vesicles with stiffer membranes confirm this hypothesis. Finally, electrofusion of vesicles with different composition was demonstrated to be an attractive approach for creating multidomain vesicles.

## Appendix: Membrane Response to Electric Fields

When vesicles are subjected to an electric field, charges accumulate at the bilayer interface creating a transmembrane potential, $V_m$, across the non-conductive membrane:[35]

$$V_m = 1.5R \cos \theta \; \mathrm{E} \left(1 - e^{-t/\tau_{charg}}\right) \tag{A.1}$$

where $R$ is the vesicle radius, E the applied electric field, $\theta$ is the angle between the electric field and the vesicle surface normal, $t$ is time, and $\tau_{charg}$ is the membrane charging time given by:[35]

$$\tau_{charg} = R \; C_m \; [1/\lambda_{in} + 1/(2\lambda_{out})] \tag{A.2}$$

Here $C_m$ is the membrane capacitance, around 1 $\mu F/cm^2$ for lipid membranes.[36,37] For the limited case of salt-free solutions and for a typical vesicle radius $R = 15$ $\mu m$, $\tau_{charg} \sim 415$ $\mu s$. For the various conductivity conditions $\lambda_{in}$ and $\lambda_{out}$, and for the different vesicle radii $R$ discussed in this work, the charging times range between 10 and 560 $\mu s$.

The transmembrane potential $V_m$ (see Eq. A.1) causes an increase in the membrane lateral tension. This contribution, also called electric tension $\sigma_{el}$, is expressed in terms of $V_m$ as:[36,38]

$$\sigma_{el} = \varepsilon\varepsilon_o \; (h \, / \, 2h_e^{\,2}) \; V_m^{\,2} \tag{A.3}$$

where $\varepsilon$ is the dielectric constant of the aqueous solution, $\varepsilon_o$ the vacuum permittivity, $h \sim 39$ Å is the total bilayer thickness, and $h_e \sim 28$ Å the dielectric thickness, both measured for lecithin bilayers.[39] Electroporation occurs when the lateral tension exceeds the membrane lysis tension $\sigma_{lys}$ (for lipid membranes $\sigma_{lys}$ is typically 6 dyn/cm), see Refs. 28 and 36. For initially tense-free vesicle, this implies creating a critical transmembrane potential $V_c \sim 1$ V. If the vesicle has some initial tension, then $V_c$ will be lower, as poration will occur whenever the total vesicle tension, which is the sum of the initial tension and the electric tension, reaches $\sigma_{lys}$.

## References

1.  V. Noireaux and A. Libchaber, *Proc. Nat. Acad. Sci. U.S.A.* **101**, 17669 (2004).
2.  A. Fischer, A. Franco and T. Oberholzer, *ChemBioChem*, **3**, 409 (2002).

3.  R. Lipowsky and R. Dimova, *J. Phys.: Condens. Matter.* **15**, S31 (2003).
4.  C. Dietrich, L. A. Bagatolli, Z. N. Volovyk, N. L. Thompson, M. Levi, K. Jacobson and E. Gratton, *Biophys. J.* **80**, 1417 (2001).
5.  T. Baumgart, S. T. Hess and W. W. Webb, *Nature* **425**, 821 (2003).
6.  S. L. Veatch and S. L. Keller, *Biophys. J.* **85**, 3074 (2003).
7.  N. Kahya, D. Scherfeld, K. Bacia, B. Poolman and P. Schwille, *J. Cell Biol*. **278**, 28109 (2003).
8.  R. Jahn and H. Grubmüeller, *Curr. Opin. Cell Biology* **14**, 488 (2002).
9.  P.L. Luisi and P. Walde (eds.), Giant vesicles. (John Wiley & Sons, Ltd. Chichester, 2000).
10. R. Dimova, S. Aranda, N. Bezlyepkina, V. Nikolov, K. A. Riske and R. Lipowsky, *J. Phys.: Condens. Matter.* **18**, S1151 (2006).
11. E. Evans and W. Rawicz, *Phys. Rev. Lett.* **17**, 2094 (1990).
12. R. Merkel, P. Nassoy, A. Leung, K. Ritchie and E. Evans, *Nature* **397**, 50 (1999).
13. A. Ashkin, *Phys. Rev. Lett*. **24**, 156 (1970).
14. R. Dimova, B. Pouligny and C. Dietrich, *Biophys. J*. **79**, 340 (2000).
15. U. Zimmermann, *Biochim. Biophys. Acta*. **694**, 227 (1982).
16. A. Richard, V. Marchi-Artzner, M.-N. Lalloz, M.-J. Brienne, F. Artzner, T. Gulik, M.-A. Guedeau-Boudeville, J.-M. Lehn, *Proc. Nat. Acad. Sci. U.S.A*. **101**, 15279 (2004).
17. C. K. Haluska, K. A. Riske, V. Marchi-Artzner, J.-M. Lehn, R. Lipowsky and R. Dimova, *Proc. Natl Acad. Sci. U.S.A.* (2006) *in press*.
18. J. C. Shillcock and R. Lipowsky, *Nature materials* **4**, 225 (2005).
19. E. Neumann, A. Sowers and C. Jordan (eds.), Electroporation and electrofusion in cell biology. (Plenum, New York, 1989).
20. D. C. Chang, B. M. Chassey, J. A. Saunders and  A. E. Sowers (eds), Guide to electroporation and electrofusion. (Academic Press, New York. 1992).
21. U. Zimmermann and G.A. Neil (eds.), Electromanipulation of cells. (CRC Press, Boca Raton, 1996).
22. K. Kinosita, Jr. and T.Y. Tsong, *Biochim. Biophys. Acta*. **471**, 227 (1977).
23. D. V. Zhelev and D. Needham, *Biochim. Biophys. Acta* **1147**, 89 (1993).
24. O. Sandre, L. Moreaux and F. Brochard-Wyart, *Proc. Natl. Acad. Sci. U.S.A*. **96**, 10591 (1999).
25. E. Tekle, R.D. Astumian, W.A. Friauf and P.B. Chock, *Biophys. J*. **81**, 960 (2001).
26. H. Aranda-Espinoza, H. Bermudez, F.S. Bates and D.E. Discher, *Phys. Rev. Lett.* **20**, 208301 (2001).
27. M.I Angelova and D.S. Dimitrov, *Faraday Discuss. Chem. Soc*. **81**, 303 (1986).
28. K. A. Riske and R. Dimova, *Biophys. J*. **88**, 1143 (2005).
29. K. A. Riske and R. Dimova, *Biophys. J*. **91**, 1778 (2006).
30. M. Mutz and H. Helfrich, *J. Phys. France* **51**, 991 (1990).
31. M. B. Schneider, J. T. Jenkins and W. W. Web, *Biophys. J*. **45**, 891 (1984).
32. K. Simons and E. Ikonen, *Nature* **387**, 569 (1997).
33. J. Korlach, P. Schwille, W. W. Webb and G. Feigenson, *Proc. Natl Acad. Sci. U.S.A.* **96**, 8461 (1999).
34. A. Roux, D. Cuvelier, P. Nassoy, J. Prost, P. Bassereau and B. Goud, *The EMBO Journal* **24**, 1537 (2005).
35. K. Kinosita, Jr., I. Ashikawa, N. Saita, H. Yoshimura, H. Itoh, K. Nagayama and A. Ikegami, *Biophys. J*. **53**, 1015 (1988).
36. D. Needham and R.M. Hochmuth, *Biophys. J*. **55**, 1001 (1989).
37. G. Cevc (ed.), Phospholipids handbook (Marcel Dekker, Inc. New York, 1993).
38. I. G. Abidor, V.B. Arakelyan, L.V. Chernomordik, Y.A. Chizmadzhev, V.F. Pastushenko and M.R. Tarasevich, *J. Electroanal. Chem*. **104**, 37 (1979).
39. S. A. Simon and T.J. McIntosh, *Methods Enzymol*. **127**, 511 (1986).